Flexible and Printed Electronics

RECEIVED
31 March 2021

REVISED
25 April 2021

ACCEPTED FOR PUBLICATION
20 May 2021

PUBLISHED
15 June 2021

PAPER

Screen-printable and flexible in-plane micro-supercapacitors with fractal electrode design

Lu Yang, Feiyao Yang, Ke Li, Wei Shen, Tao Xu, Xiaobing Xu, Yaning Zhou, Mengjuan Zhong, Mingchuan Zheng and Di Wei*

Beijing Graphene Institute, Beijing 100095, People's Republic of China
* Author to whom any correspondence should be addressed.

E-mail: diwei@hotmail.com

Keywords: micro-supercapacitors, screen printing, fractal electrode design, Hilbert curve

Supplementary material for this article is available online

Abstract

New microscale energy devices need to be developed to accommodate the evolution of integrated flexible electronic systems. Supercapacitors have the advantages of high power density and long cycle life, and can be used independently or combined with batteries to provide electric energy for future electronics. Screen printing is a simple, cost-effective method for fast and scalable fabrication of micro-supercapacitors (MSCs) on various types of substrates that does not involve complicated process or expensive equipment. Currently, most researches of MSCs have been focused on materials and ink development with conventional interdigital architecture, few studies have been aimed at electrode pattern design. Herein, we demonstrate an in-plane MSCs via screen printing with designable electrode patterns on flexible substrate. The thickness of the device is less than 1 mm, ensuring good flexibility. By replacing the carbon ink with the silver ink as current collectors, the performance is improved due to lower device resistance. Owing to the geometric controllability of the screen printing method, we are able to study the effects of electrode design on the output performance by simply changing the screen mesh patterns. In particular, we demonstrate that by adapting the mathematical fractal concept such as Hilbert curve as electrode patterns, the areal capacitance of MSCs can reach up to 28.7 mF cm^{-2}, which is 46.8% higher than that of the traditional interdigital structure. The results suggest that the fractal-based design represents a universal protocol for producing MSCs. Without changing electrode materials or fabrication facilities, the design strategy is highly compatible with industrial scale screen printing for roll-to-toll processing. This high-capacitance, cost-effective and flexible MSCs open a promising pathway for providing electric energy for the Internet of Things and future wearable systems.

1. Introduction

Energy storage devices are critical for the integrated electronic systems. The development of the flexible miniature electronics such as electronic skins [1], wearable health monitors [2] and sensors for the Internet of Things [3] highlights the demand of microscale energy storage devices [4]. Various electrochemical energy storage technologies have been investigated to achieve miniaturization, like 3D lithium-ion microbatteries [5] and printed zinc-silver oxide batteries [6]. Different from conventional batteries, micro-supercapacitors (MSCs) store energy through reversible ion adsorption or redox reactions on the electrode surface, and have the advantages of high power density and long cycle life [7] thus can complement batteries or be used independently as power sources. The supercapacitors with traditional nonplanar stacked configuration have shown high capacitance and high energy density, however, they suffer from bulky volume, fixed shape and poor integrity of electrode films from cracking and delamination when used for flexible applications [8, 9]. The MSCs with in-plane geometries are free

of separators and relatively thin, therefore can better meet the demand of flexibility for portable and wearable microelectronics.

A variety of fabrication methods such as electrophoretic deposition [10, 11], photolithography [9] and laser scribe [8, 12] have been explored to produce MSCs. However, these technologies require complicated procedure, expensive equipment and lengthy processing time, therefore are not suitable for large-scale production. Alternatively, screen printing is a simple and cost-effective method that used extensively in industry to print text and images [13]. It has the intriguing feature of geometric controllability by simply changing the screen mesh patterns [14, 15]. This scalable printing technique is also compatible with diverse inks and substrate materials and is promising for printing micro-batteries and MSCs with roll-to-toll processing [16].

To date, great progress has been made to produce MSCs, focusing on developing nanostructured electrode materials such as capacitive nanocarbons [9, 10], 2D graphene [17–19], conductive polymers [20, 21] and pseudocapacitive metal oxides [22, 23]. Despite the enormous advancements, most of these researches use the conventional interdigital architecture, few have studied the effects of the electrode structure design on the output performance of MSCs. Tiliakos *et al* [24] fabricated a supercapacitors carpets with graphene forms by the laser printing method with the capacitance up to 6.1 mF cm^{-2} and investigated the architectures factors that affect the performance. Huang *et al* [25] presented buckypaper-based MSCs via a standard lithography process and vacuum-filtration and optimized the fractal electrode design to improve the capacitance to 18.82 mF cm^{-2}. These studies have shown encouraging results that the performance of MSCs can be improved by careful electrode design. However, the complicated fabrication process hinders their further application.

Herein, we report a flexible in-plane MSCs with designable electrode patterns via screen printing. The device shows good flexibility with the total thickness of less than 1 mm. The capacitance is optimized by replacing carbon current collectors with silver to reduce the internal resistance. To study the impact of electrode patterns on the output performance, MSCs with fractal electrode design are fabricated to compare with MSCs with interdigital electrode structures by simply changing the patterns on the screen printing meshes. The fractal geometry is a mathematical concept, in which space filling curves like Hilbert curves and Peano curves can completely fill up a finite area with an infinite continuous curve. The space filling curves in fractals have the self-similarity property, meaning similar fine structures can be observed at any magnification scale, thus increasing the complexity of the structure. It has been employed by electronic circuit to increase the stretchability [26], by semiconductors to build transparent electrodes [27], by antennas for broadband near-field concentration [28] and by moisture-enabled power sources to improve the power density [29]. In capacitors, it is reported that corners and edges are able to store more charges than a planar surface [25], therefore, it is possible to increase the capacitance by utilizing complex fractal pattern design. In this work, we adapt the Hilbert space filling curve with different level of complexity as the electrode patterns and studied their influence on the MSCs capacitance. With the increasing of complexity, the MSCs show decreasing internal resistance and increasing area capacitance. Comparing to MSCs with the interdigital structure, MSCs with the fractal architecture using same active material, line width and electrode distance have the areal capacitance of 28.7 mF cm^{-2}, which is 46.8% higher than that of the interdigital structure. This study indicates that fractal electrode design is an effective way to improve the performance of MSCs and is highly compatible with the geometric controllability of the screen printing technique, providing a simple method to produce flexible high-capacitance in-plane MSCs. Without changing the active material, electrode inks or fabrication process, this design strategy is suitable for the current industrial scale roll-to-roll processing to provide electrical energy for the Internet of Things and wearable electronics.

2. Experimental

2.1. Materials and ink preparation

The commercial activated carbon (YP-50F, Kuraray, Japan) was chosen as active material for composite electrodes. Carbon black, polyvinylidene fluoride (PVDF) and *N*-methyl-2-pyrrolidone (NMP) were purchased from MTI Corp. and used as conductive additive, binder and solvent respectively. Conductive carbon ink and silver ink were purchased from Chang Sung Corporation and used as received.

To prepare the electrode ink, activated carbon (80 wt.%), carbon black (10 wt.%) and PVDF (10 wt.%) were added into NMP and mixed with a planetary centrifugal mixer (Mazerustar, Japan), forming a stable viscous ink. For gel electrolyte, polyvinyl alcohol (PVA 1799) solution was prepared by dissolving PVA polymer in deionized water at 85 °C for 2 h under magnetic stirring, then H_3PO_4 was slowly added into PVA solution with weight ratio of 1:1 regarding PVA polymer, forming H_3PO_4/PVA gel electrolyte.

2.2. Screen printing and device fabrication

The printing process was carried out by the bench-top semi-automatic screen printing film coater (EQ-SPC-3050, MTI Corp.) on a flexible polyethylene terephthalate (PET) film substrate. The position adjustment accuracy of the machine is ±0.08 mm. The screen mold was made of standard polyester fibers with the mesh count of 200 mesh/inch and the thread diameter

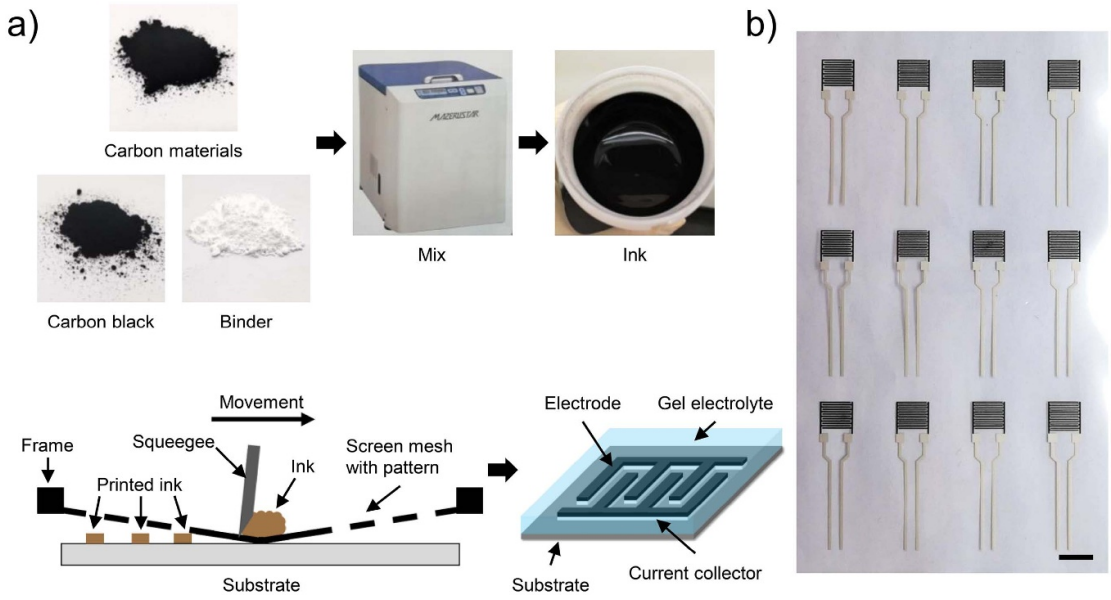

Figure 1. Fabrication of MSCs. (a) Schematics of the ink preparation process and the fabrication process of MSCs. Electrode materials are mixed uniformly with the solvent forming a stable viscous electrode ink. Patterned current collectors, electrodes are subsequently deposited onto the flexible substrate via screen printing. Gel electrolytes are then drop casted onto the printed area. (b) Photograph of screen-printed MSCs. Scale bar: 1 cm.

of 55 μm. Through a direct stencil making process with the sensitive emulsion, a patterned screen mesh was made by exposing the lithographic film which has the resolution of 24 000 dpi. For the printing process, first, the conductive carbon or silver ink was printed onto PET and cured at 120 °C for 30 min forming patterned current collectors. Then, the electrode ink was printed directly onto current collectors and dried at 80 °C in vacuum oven for overnight. The gel electrolyte H_3PO_4/PVA was then drop casted onto PET to cover the electrode area and solidified at 40 °C for 5 h. Finally, the as obtained MSCs were sealed between laminating films to protect the devices.

2.3. Characterization

The viscosity of the electrode ink was measured by the rheometer (Discovery, DHR-2) in parallel plate geometry at 25 °C. Optical microscope images were obtained by an industrial microscope (LV100ND, Nikon, Japan). The microstructure of the samples was examined using the scanning electron microscope (SEM, FEI Quattro S) with a 10 kV accelerating voltage. The thickness of the printed layer was measured by the digimatic indicator (Absolute 543-490B, Mitutoyo Corp.). All electrochemical measurement was conducted by the electrochemical workstation (Metrohm Multi Autolab M204) with the two-electrode setup at room temperature. Cyclic voltammetry (CV) tests were carried out with different scan rate of 1, 2, 5, 10, 20, 50, 100 mV s^{-1} within the voltage window of 0–0.8 V. Galvanostatic charge discharge (GCD) tests were conducted at different current densities from 0.005 to 0.13 mA cm^{-2}. Electrochemical impedance spectroscopy (EIS) tests were recorded in the frequency range from 0.01 to 100 kHz with the amplitude of 10 mV at open circuit voltage.

3. Results and discussion

3.1. Ink preparation and MSCs fabrication

The schematics of the ink preparation and device fabrication process are illustrated in figure 1. The activated carbon is chosen as active material since it is a readily available electrode material for electric double layer capacitors (EDLC) and is widely used in commercial supercapacitors. The electrode ink is composed of active materials, conductive additives and polymer binders, which are mixed uniformly in the NMP solvent, forming a stable viscous ink. The viscosity of the ink is a critical parameter for the screen printing process and is adjusted by the solvent content. If the content of solvent is too high, the ink viscosity will decrease, resulting in spreading inks and blurred printed patterns on the substrate. If the content of solvent is too low, the ink viscosity will increase, leading to nonuniform material distribution and blockage of the screen mesh. The printable electrode ink in this study has 75 wt.% NMP solvent and has shear-thinning behavior as shown in figure SI1 (available online at stacks.iop.org/FPE/6/025008/mmedia), which is favorable for the screen printing process since it allows extrusion through screen meshes under the shear force and then quick solidification once the printing is finished.

The screen printing process is shown in figure 1(a). The insulating substrate is placed below the patterned screen and the ink is extruded through

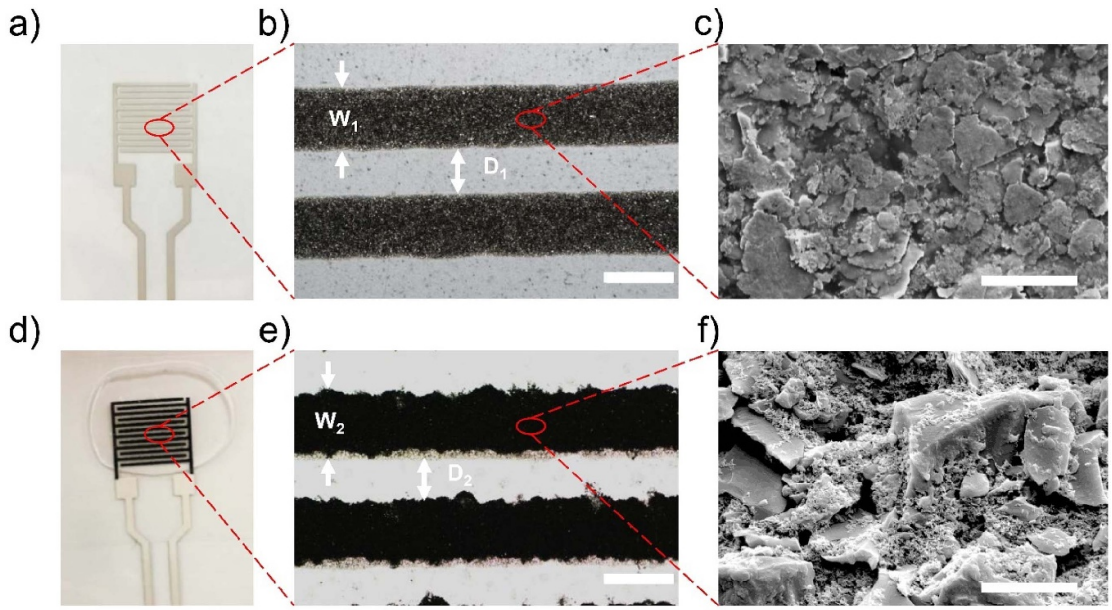

Figure 2. Images of printed interdigital silver current collectors and MSCs. (a) The photo of interdigital silver current collectors. (b) The optical microscope image of silver lines shows that the line width (W_1) is (0.49 ± 0.03) mm and the distance between lines (D_1) is (0.29 ± 0.01) mm. Scale bar: 0.5 mm. (c) The SEM image of silver inks shows nanoparticles with no obvious agglomeration. Scale bar: 10 μm. (d) The photo of interdigital MSCs with silver current collectors. (e) The optical microscope image of the interdigital MSCs shows good alignment of electrode and silver layers. The line width (W_2) is (0.51 ± 0.02) mm and the distance between lines (D_2) is (0.30 ± 0.01) mm. Scale bar: 0.5 mm. (f) The SEM image of electrode inks shows microstructures with uniform particle distribution. Scale bar: 10 μm.

the screen mesh for deposition onto the placed substrate. It should be noted that this method is universal for a wide range of materials and substrates and has outstanding geometric controllability. The resolution is mainly determined by the screen meshes and the thickness of the printed layer varies with the repeating times of printing. Through mesh pattern design, complex planar geometries can be obtained with relatively good precision within seconds by one-step screen printing and the printed patterns exhibit large-area uniformity and batch-to batch reproducibility (figure 1(b)). After drying of the electrodes, the gel electrolyte H_3PO_4/PVA is drop-casted and then the device is sealed. The obtained all-solid-state MSCs have the total thickness of less than 1 mm including the sealing and exhibit excellent flexibility.

3.2. Electrochemical performance of interdigital MSCs

To demonstrate the adaptability of printing process, interdigital MSCs with carbon ink and silver ink as current collectors are fabricated establishing references of electrochemical performance. Carbon ink is a conductive ink that widely used in printing industry for chip components, flexible printed circuit boards and electronic control units. It is a low-cost and environmentally friendly ink suitable for screen printing. However, the electrical conductivity is limited comparing to that of metal conductive inks. Therefore, silver ink is also tested as current collectors since it has higher conductivity and has been used for many active materials for supercapacitor applications [17, 30, 31]. The images of printed carbon and silver current collectors and interdigital MSCs are shown in figures SI2 and 2. The designed line width and distance between lines of interdigital electrodes are 0.4 mm and the total printing area is 1 cm^2. This electrode distance is mainly limited by the precision of the pilot screen printer in laboratory for good batch reproducibility and avoiding short circuits. The geometry of the actual printed pattern deviates slightly from the screen mesh design due to the spreading of printed inks. For printed silver current collectors, the line width (W_1) is (0.49 ± 0.03) mm and the distance between lines (D_1) is (0.29 ± 0.01) mm (figure 2(b)). For interdigital MSCs with silver current collectors, the alignment of the electrode layer and the current collector layer are relatively good (figure 2(e)), and the line width (W_2) is (0.51 ± 0.02) mm and the distance between lines (D_2) is (0.30 ± 0.01) mm. The thickness of the current collector layer, electrode layer and electrolyte layer are 9, 30 and 350 μm respectively. The SEM images of carbon and silver inks show no obvious nanoparticle agglomeration (figures SI2 and 2(c)). The microstructure of the printed electrode layer shows uniformly distributed activated carbon particles, carbon blacks and polymer binders (figure 2(f)).

The electrochemical performance of MSCs with carbon and silver current collectors is evaluated by CV, GCD and EIS as shown in figures SI3 and 3.

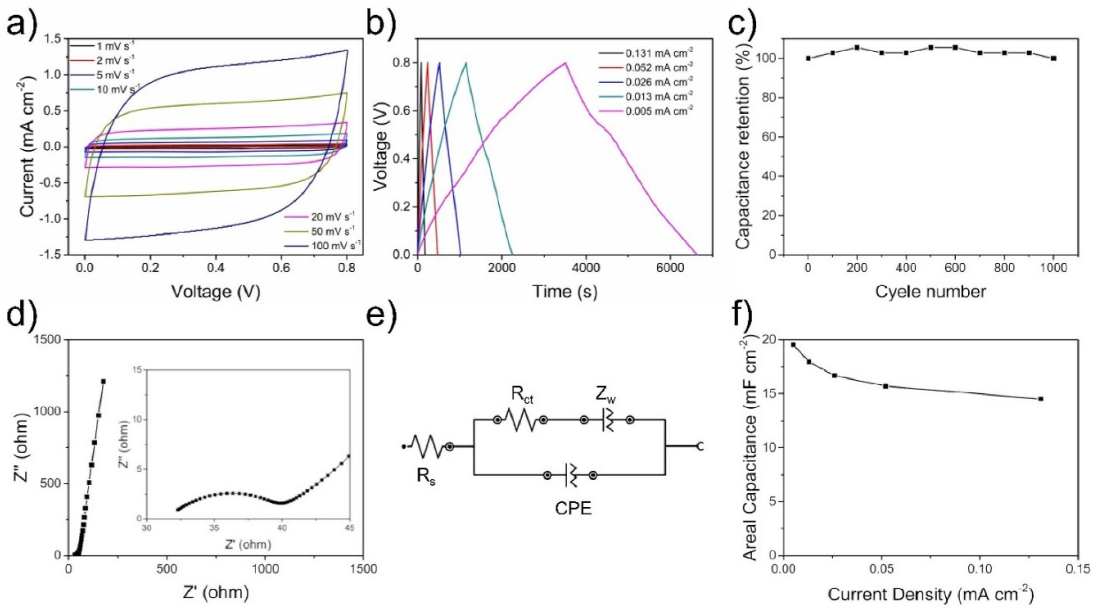

Figure 3. Electrochemical performance of interdigital MSCs with silver current collectors. (a) CV test results at different scan rates. (b) GCD profiles tested at different current densities. (c) Cycling stability at the current density of 0.1 mA cm^{-2} for 1000 cycles. (d) The complex plane plot obtained by EIS. (e) The equivalent circuit model for EIS tests. (f) The areal capacitance at different current densities.

The discussion of the electrochemical performance of MSCs with carbon current collectors is detailed in the supplementary information (figure SI3). For interdigital MSCs with silver current collectors, to avoid released silver ions penetrating electrolytes and participating the electrochemical reactions, the activated carbon layer and silver current collectors are carefully aligned to reduce silver exposure. The CV curves of MSCs are near rectangular in shape at low scan rate with no obvious redox reaction peaks indicating typical EDLC behavior, which mainly comes from the activated carbon (figure 3(a)). We have also carried out CV tests of silver interdigital electrodes in direct contact with the electrolyte without the activated carbon layer to eliminate the capacitance from current collectors. As shown in figure SI4, the response current is relatively small compare to that of the MSCs and there are no obvious redox peaks, meaning the silver particles contribute very little to the total capacitance of MSCs. The GCD profiles of MSCs in figure 3(b) shows near symmetrical charge and discharge profiles indicating typical EDLC behavior, which is consistent with the CV results. The MSCs also display cycling stability with no apparent capacitance degradation after 1000 GCD cycles at 0.1 mA cm^{-2} (figure 3(c)).

To evaluate the internal resistance of the MSCs, EIS measurement is performed at open circuit voltage from 0.01 Hz to 100 kHz. As shown in figure 3(d), the Nyquist plot obtained from the MSCs with silver current collectors exhibits a semicircle at high frequencies and a straight tail at low frequencies, which is a typical capacitive behavior. The semicircle in the complex plane represents the charge transfer process at the interface between the electrode and electrolyte. The nearly vertical line along the imaginary axis at low-frequency region represents the diffusion of ions in the electrolyte. The equivalent circuit model for EIS test is shown in figure 3(e). R_s represents the equivalent series resistance (ESR) including the total resistance of the electrode, electrolyte, and the current collectors, which is obtained from the intercept of the Nyquist plot on the real axis within the high-frequency region. R_{ct} is the charge transfer resistance obtained from the diameter of the semicircle. The constant phase element (CPE) accounts for the electric double layer capacitance and the Warburg element (Z_w) represents the frequency dependence of ion diffusion and transportation in the electrolyte. The ESR of MSCs with silver current collectors is around 30 Ω, which is significantly lower than 1500 Ω for MSCs with carbon current collectors (figure SI3). This is consistent with the resistance measurement of the printed silver strip (1 Ω cm^{-1}) and the carbon strip (50 Ω cm^{-1}) with the same thickness. The areal capacitance of the MSCs with silver current collectors calculated from GCD tests can reach up to 19.5 mF cm^{-2} and does not decrease much with increasing current density and is higher than that of MSCs with carbon current collectors at all tested current densities (figure 3(f)). These results reveal that the interdigital MSCs with silver current collectors has significantly lower internal resistance due to the higher electrical conductivity of silver inks, leading to increasing areal capacitance and better output performance.

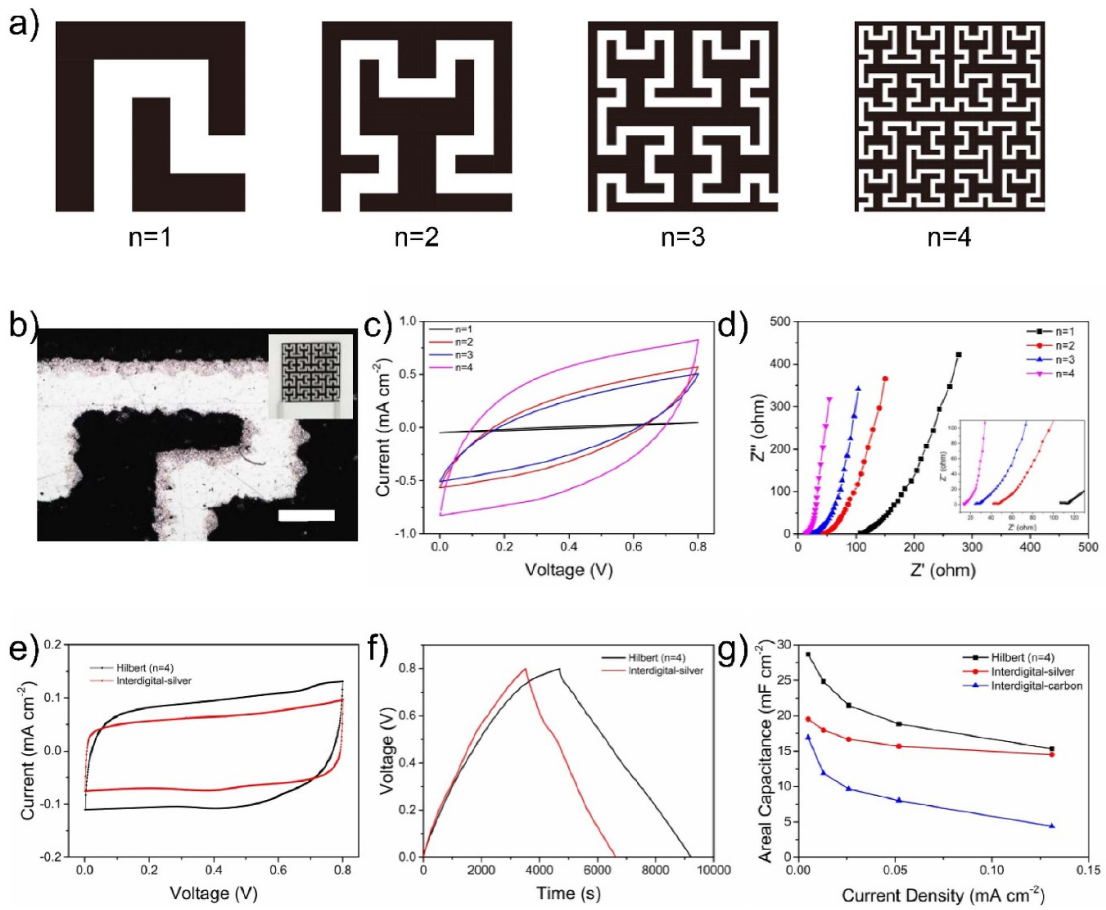

Figure 4. MSCs with fractal electrode design. (a) Illustration of the MSCs electrode pattern design adapted from the Hilbert curve with different iterations ($n = 1, 2, 3, 4$). The area is divided by a continuous curve (white) into two regions (black) which are filled with printed electrode inks. (b) The optical microscope image of the fractal MSCs ($n = 4$) with silver current collectors. Scale bar: 0.5 mm. The insert is the photo of the printed fractal MSCs ($n = 4$). (c) CV test results of fractal MSCs with different iterations at the scan rate of 50 mV s^{-1}. (d) The EIS test results of fractal MSCs with different iterations. (e) CV comparison of interdigital MSCs and fractal MSCs ($n = 4$) with same designed line width and distance at the scan rate of 5 mV s^{-1}. (f) GCD profiles of interdigital MSCs and fractal MSCs ($n = 4$) tested at the current density of 0.005 mA cm^{-2}. (g) The areal capacitance comparison of MSCs with different electrode patterns and current collectors at different current densities.

3.3. Fractal electrode design

Besides the electrode materials and current collectors, the pattern design of the electrodes also has great impact on the output performance of MSCs. It is reported that the electrode structures with corners or edges can accommodate more charges than those with a planar surface, which might be attributed to larger effective electrode volume [25, 32, 33]. Therefore, higher capacitance MSCs could be achieved through carefully designed electrode architectures with increasing complexity. The space-filling curve in fractal geometry is a mathematical concept that defines the curves with infinity length that pass through every point of a finite region. It is a continuous curve with complex structures formed by repeatedly copying and shrinking a unit line segment. In this work, owing to the geometric controllability of screen-printing method, Hilbert curve can be adapted as the fractal electrode patterns for the printed MSCs to study the effect of electrode design on the output performance by simply changing the patterns on the screen meshes. By increasing the iteration of the Hilbert curve, the entire 2D space can be filled with a continuous self-similar curve and the shape complexity can increase exponentially. The curve also has the intriguing property of splitting the area into two separate regions, which can be filled with inks as two continuous electrodes for MSCs.

As shown in figure 4(a), Hilbert curves with increasing iteration ($n = 1, 2, 3, 4$) are adapted as electrode patterns. The black area represents the electrode region of MSCs, and the white area in the shape of Hilbert curve is the space that separates two electrodes. The detailed characteristics of the pattern design are listed in table 1. The side length is 1.6 cm and the device area is 2.56 cm^2 for all four fractal patterns. The line width is equal to the distance between lines in each pattern, and decreases with increasing iteration. The slot length increases with increasing iteration, while the slot area and electrode area ratio remain the same, since similar fine structures can be observed at any magnification scale. It should be

Table 1. Characteristics of MSCs pattern design.

Pattern design	Line width (mm)	Side length (mm)	Slot length (mm)	Slot area (%)	Electrode area (%)
Hilbert ($n = 1$)	3.2	16	28.8	36	64
Hilbert ($n = 2$)	1.6	16	57.6	36	64
Hilbert ($n = 3$)	0.8	16	115.2	36	64
Hilbert ($n = 4$)	0.4	16	230.4	36	64
Interdigital	0.4	10	114.8	46	54

noted the fractal design with iteration $n = 4$ has similar designed line widths and distance with that of the interdigital structures. However, the slot area ratio of the fractal design is 36%, smaller than 46% for the interdigital structure, meaning more area filled with electrode inks. Also, the fractal pattern has more corners and edges than the interdigital structure.

The optical microscope images of the printed fractal MSCs are shown in figures 4(b) and SI5. The printed pattern shows relatively good alignment and precision. As mentioned before, in a confined area, with increasing iteration, the line width and electrode distance will decrease while the degree of architectural complexity will increase dramatically. For the MSCs fabricated via screen printing (figure SI6), the line width is mainly limited by the precision of our lab pilot screen printer, since the alignment error of the electrode and current collector layer introduced by manual adjustment might cause short circuit. The iteration could be further increased by industrial screen printer. The automatic screen printing machine with precise mechanical control system used for batch production could reduce the risk of short circuit and enable smaller line widths and gaps in complex patterns.

The electrochemical performance of fractal MSCs is evaluated by CV, GCD and EIS tests. The CV curves of MSCs with different iteration at 50 mV s^{-1} show that the responding current and the area of the curves increase with increasing iteration (figure 4(c)), indicating increasing capacitance with higher iteration. The CV curve of MSCs with iteration $n = 4$ exhibits a typical EDLC behavior which agrees with GCD tests carried out at different current densities (figure SI7). The shape of the EIS test results is similar to that of interdigital MSCs with a semicircle and a straight tail, therefore could be evaluated with the same equivalent circuit. The ESR of the fractal MSCs obtained from the intercept of the Nyquist plot on the real axis decreases with increasing iteration (figure 4(d)), meaning lower internal resistance with higher iteration. The difference in capacitance and internal resistance comes from the geometric design of the fractal MSCs. Although the slot area of the fractal patterns is the same, the line widths and slot lengths of the MSCs are different for each pattern. With increasing iteration, the line width decreases from 3.2 to 0.4 mm, indicating shorter ion transportation distance between two electrodes. Also, the structural complexity increases dramatically with higher iteration, which could lead to higher charge storage capacity. These tests demonstrate that for the fractal MSCs in a confined area, by increasing the iteration, the capacitance could be improved due to decreasing internal resistance and increasing structure complexity.

To stress the importance of pattern design strategy, the electrochemical performance of the MSCs with interdigital structures is compared with that of the fractal MSCs. As shown in figures 4(e) and (f), fractal MSCs ($n = 4$) shows larger CV curve area and longer charge and discharge time, indicating higher capacitance. The areal capacitance of fractal MSCs ($n = 4$) is calculated from the GCD profiles and compared with the interdigital MSCs with different current collectors (figure 4(g)). The areal capacitance of fractal MSCs can reach up to 28.7 mF cm^{-2}, which is 46.8% higher than that of the interdigital structure with silver current collectors and the same electrode materials. Since the fractal design with iteration $n = 4$ has similar electrode distance with that of the interdigital structures, their electrochemical performance is comparable without the influence of the ion transportation distance. As shown in table 1, the electrode area of the fractal design is 64%, higher than 54% for the traditional interdigital pattern, meaning more active materials loading in a unit area. In addition, the complex fractal structure contains more corners and edges, which might also contribute to the increasing charge storage capability. These results suggest that fractal design strategy is effective to enhance the output performance of the printed MSCs.

4. Conclusion

In this work, we fabricate an in-plane MSCs with designable electrode patterns via screen printing. The device has the thickness of less than 1 mm, exhibiting good flexibility. By replacing the carbon ink with silver ink as current collectors, the output performance is improved due to lower internal resistance. To study the effect of complex electrode structures on capacitance, MSCs with fractal design are printed by simply changing the patterns on the screen mesh. The Hilbert space filling curve is adapted as electrode design and the area capacitance of the fractal MSCs can reach up to 28.7 mF cm^{-2}, 46.8% higher than that of the interdigital structure, indicating that

increasing the degree of complexity of electrode structures is an effective way to improve the capacitance for MSCs. The output performance could be further tailored through interconnecting MSCs in parallel, in series and in arbitrary arrangements [34]. The MSCs could also be printed on both sides of the flexible substrate to improve space utilization. The geometric controllability of screen printing method combined with the fractal design strategy shows great potential for scalable production of flexible MSCs for powering the electronic devices.

Data availability statement

All data that support the findings of this study are included within the article (and any supplementary files).

Acknowledgments

This work was supported by Beijing Municipal Science & Technology Commission No. Z181100004818004, No. Z181100001018029 and No. Z191100006119027. The authors also appreciate the technical assistance from the Beijing Graphene Institute Characterization & Quality Assurance Center.

ORCID iD

Di Wei https://orcid.org/0000-0003-2670-6362

References

[1] Hammock M L, Chortos A, Tee B C K, Tok J B H and Bao Z 2013 25th anniversary article: the evolution of electronic skin (E-Skin): a brief history, design considerations, and recent progress *Adv. Mater.* **25** 5997–6038
[2] Zhang L *et al* 2020 Micro-nano hybrid-structured conductive film with ultrawide range pressure-sensitivity and bioelectrical acquirability for ubiquitous wearable applications *Appl. Mater. Today* **20** 100651
[3] Gubbi J, Buyya R, Marusic S and Palaniswami M 2013 Internet of Things (IoT): a vision, architectural elements, and future directions *Future Gener. Comput. Syst.* **29** 1645–60
[4] Liu H, Zhang G, Zheng X, Chen F and Duan H 2020 Emerging miniaturized energy storage devices for microsystem applications: from design to integration *Int. J. Extreme Manuf.* **2** 042001
[5] Sun K, Wei T-S, Ahn B Y, Seo J Y, Dillon S J and Lewis J A 2013 3D printing of interdigitated Li-ion microbattery architectures *Adv. Mater.* **25** 4539–43
[6] Kumar R, Shin J, Yin L, You J-M, Meng Y S and Wang J 2017 All-printed, stretchable Zn-Ag_2O rechargeable battery via hyperelastic binder for self-powering wearable electronics *Adv. Energy Mater.* **7** 1602096
[7] Du Pasquier A, Plitz I, Menocal S and Amatucci G 2003 A comparative study of Li-ion battery, supercapacitor and nonaqueous asymmetric hybrid devices for automotive applications *J. Power Sources* **115** 171–8
[8] El-Kady M F, Strong V, Dubin S and Kaner R B 2012 Laser scribing of high-performance and flexible graphene-based electrochemical capacitors *Science* **335** 1326–30
[9] Huang P *et al* 2016 On-chip and freestanding elastic carbon films for micro-supercapacitors *Science* **351** 691–5
[10] Pech D, Brunet M, Durou H, Huang P, Mochalin V, Gogotsi Y, Taberna P-L and Simon P 2010 Ultrahigh-power micrometre-sized supercapacitors based on onion-like carbon *Nat. Nanotechnol.* **5** 651–4
[11] Zhang G *et al* 2021 Integrating flexible ultralight 3D Ni micromesh current collector with NiCo bimetallic hydroxide for smart hybrid supercapacitors *Adv. Funct. Mater.* 2100290
[12] El-Kady M F and Kaner R B 2013 Scalable fabrication of high-power graphene micro-supercapacitors for flexible and on-chip energy storage *Nat. Commun.* **4** 1475
[13] Liu N and Gao Y 2017 Recent progress in micro-supercapacitors with in-plane interdigital electrode architecture *Small* **13** 1701989
[14] Shi X, Pei S, Zhou F, Ren W, Cheng H-M, Wu Z-S and Bao X 2019 Ultrahigh-voltage integrated micro-supercapacitors with designable shapes and superior flexibility *Energy Environ. Sci.* **12** 1534–41
[15] Liang J, Feng Y, Liu L, Li S, Jiang C and Wu W 2019 All-printed solid-state supercapacitors with versatile shapes and superior flexibility for wearable energy storage *J. Mater. Chem.* A **7** 15960–8
[16] Gaikwad A M, Arias A C and Steingart D A 2015 Recent progress on printed flexible batteries: mechanical challenges, printing technologies, and future prospects *Energy Technol.* **3** 305–28
[17] Liu S, Xie J, Li H, Wang Y, Yang H Y, Zhu T, Zhang S, Cao G and Zhao X 2014 Nitrogen-doped reduced graphene oxide for high-performance flexible all-solid-state micro-supercapacitors *J. Mater. Chem.* A **2** 18125–31
[18] Zhou F *et al* 2018 Electrochemically scalable production of fluorine-modified graphene for flexible and high-energy ionogel-based microsupercapacitors *J. Am. Chem. Soc.* **140** 8198–205
[19] Bellani S, Petroni E, Del Rio Castillo A E, Curreli N, Martín-García B, Oropesa-Nuñez R, Prato M and Bonaccorso F 2019 Scalable production of graphene inks via wet-jet milling exfoliation for screen-printed micro-supercapacitors *Adv. Funct. Mater.* **29** 1807659
[20] Xu Y, Schwab M G, Strudwick A J, Hennig I, Feng X, Wu Z and Müllen K 2013 Screen-printable thin film supercapacitor device utilizing graphene/polyaniline inks *Adv. Energy Mater.* **3** 1035–40
[21] Wu Z-S, Parvez K, Li S, Yang S, Liu Z, Liu S, Feng X and Müllen K 2015 Alternating stacked graphene-conducting polymer compact films with ultrahigh areal and volumetric capacitances for high-energy micro-supercapacitors *Adv. Mater.* **27** 4054–61
[22] Cho S, Kim M and Jang J 2015 Screen-printable and flexible RuO_2 nanoparticle-decorated PEDOT:PSS/graphene nanocomposite with enhanced electrical and electrochemical performances for high-capacity supercapacitor *ACS Appl. Mater. Interfaces* **7** 10213–27
[23] Li H, Li X, Liang J and Chen Y 2019 Hydrous RuO_2-decorated mxene coordinating with silver nanowire inks enabling fully printed micro-supercapacitors with extraordinary volumetric performance *Adv. Energy Mater.* **9** 1803987
[24] Tiliakos A, Trefilov A M I, Tanas E, Balan A and Stamatin I 2018 Space-filling supercapacitor carpets: highly scalable fractal architecture for energy storage *J. Power Sources* **384** 145–55
[25] Huang K-H, Lin C-T, Chen Y-T and Yang Y-J 2019 Study of fractal electrode designs for buckypaper-based micro-supercapacitors *J. Appl. Phys.* **125** 014902
[26] Fan J A *et al* 2014 Fractal design concepts for stretchable electronics *Nat. Commun.* **5** 3266
[27] Afshinmanesh F, Curto A G, Milaninia K M, van Hulst N F and Brongersma M L 2014 Transparent metallic fractal electrodes for semiconductor devices *Nano Lett.* **14** 5068–74
[28] Sederberg S and Elezzabi A Y 2011 Sierpiński fractal plasmonic antenna: a fractal abstraction of the plasmonic bowtie antenna *Opt. Express* **19** 10456–61

[29] Yang L et al 2021 A moisture-enabled fully printable power source inspired by electric eels *Proc. Natl Acad. Sci.* **118** e2023164118
[30] Wang Y et al 2014 Printed all-solid flexible microsupercapacitors: towards the general route for high energy storage devices *Nanotechnology* **25** 094010
[31] Liu L, Tian Q, Yao W, Li M, Li Y and Wu W 2018 All-printed ultraflexible and stretchable asymmetric in-plane solid-state supercapacitors (ASCs) for wearable electronics *J. Power Sources* **397** 59–67
[32] Thekkekara L V and Gu M 2017 Bioinspired fractal electrodes for solar energy storages *Sci. Rep.* **7** 45585
[33] Moselhy T, Ghali H, Ragaie H F and Haddara H 2003 Investigation of space filling capacitors *Proc. 12th IEEE Int. Conf. Fuzzy Systems (Cat. No.03CH37442)* (*IEEE, Cairo Egypt, 2003*) pp 287–90
[34] Sun H, Fu X, Xie S, Jiang Y and Peng H 2016 Electrochemical capacitors with high output voltages that mimic electric eels *Adv. Mater.* **28** 2070–6